A Study of the Electrical Characteristics of an Oxy-Fuel Flame

Christopher Martin[a,*], Castle Leonard[a], Josh VonFricken[a]

[a] *The Pennsylvania State University, Altoona College, 3000 Ivyside Park Altoona, PA 16601*

Abstract

Electrical phenomena useful for oxy-fuel process sensing are demonstrated at signal level voltages applied to an oxy-fuel cutting torch. The current-voltage characteristic of the flame between the torch and work is recorded while varying torch-to-plate standoff, fuel-oxygen ratio, total flow rate, and plate temperature. At $\pm$10V, typical currents are on the order -100μA to 25μA, and the I-V characteristic exhibits three regimes. At low currents, the relationship between voltage and current is linear. At positive currents, transition to saturation is heavily curved around 10μA to 20μA. Negative currents do not totally saturate in this voltage range, but there is an abrupt transition to a new slope, which we describe as "partial" saturation. The properties of these regimes demonstrate strong repeatable links to standoff and fuel-oxygen ratio. Flow rate and plate temperature also demonstrate correlation to these electrical properties despite substantial scatter.

1. Introduction

In the present study, we investigate ion currents in the preheat flame of an oxy-fuel cutting torch as a potential means for sensing system parameters. While applying signal level voltages (-10V to 10V) between the torch and a metal work surface, measured currents were on the order -100μA to 25μA, and demonstrate nonlinear behaviors with sufficient complexity to potentially allow the inference of multiple important system parameters from a single electrical waveform.

1.1. Motivation

Oxy-fuel cutting is a century-old process for cutting steel uses a jet of pure oxygen located concentrically in a semi-annular preheat flame to burn away hot iron. Figure 1 shows the geometry of the Oxweld $\frac{1}{2}$-inch tip used in this investigation. The preheat flame is fed by the channels formed at the interface between a brass insert and sleeve.

*Corresponding author
Email address: crm28@psu.edu (Christopher Martin)

Figure 1: Two-piece oxy-fuel tip. (Left) The insert and sleeve are laid on a 12.7mm ($\frac{1}{2}$in) grid for scale. The preheat channels are cut into the brass insert, and flow conditioning holes are visible in the back end of the insert. (Right) The insert and sleeve are assembled and viewed from the tip. The semi-triangular channels form the preheat channels and the center bore is the cutting channel.

In normal mechanized (automated) operation, the preheat flame heats the work piece until it reaches its kindling temperature, and a transonic jet of pure oxygen is issued from the cutting channel. The preheat flame is used primarily to heat the work's surface, and it is the chemical energy released in the kerf of the cut that provides the energy necessary to perpetuate the process through the work's thickness [1].

There is substantial interest in developing a sensing suite for these systems that is both economical and robust: a task for which ion currents could be ideal. The first obstacle to such an approach is the lack of data available on flames matching this geometry under conditions appropriate to the problem.

In the present investigation, we control for four parameters of engineering interest: the standoff between the tip and the work piece, the fuel-oxygen (F/O) mixture, the total preheat flow rate, and the work surface temperature. Typical cutting standoffs may vary from 5mm to 30mm (about $\frac{1}{4}$in to 1in). The surface temperatures of interest are determined by the kindling temperature typical to steels and the melting point of the SAE 4140 steel used in this experiment. Bolobov et al. places the autoignition of steels in oxygen from 960°C to 1371°C (1760°F to 2500°F) [2], and the melting temperature of the 4140 steel coupon used in this work is reported to be approximately 1450°C (2552°F) [3].

The present investigation is limited to preheat conditions, wherein the flame is used to heat a circular coupon simulating a work piece with no cutting oxygen. Fuel-oxygen mixtures are limited to the stoichiometric-to-rich conditions typical to maximize heating.

1.2. Background

Though the history of investigations into electrical currents in flames can now be measured in centuries, these problems are sufficiently complicated as to still harbor surprising eccentricities. Because of the sophistication of the physics involved, it can be quite dangerous to generalize lessons learned in simpler systems without first verifying their validity by full-scale experiment.

At the start of the twentieth century, describing electrical phenomena in flames with the motion of charged particles was quite new [4]. Measurements of tiny currents between wire electrodes in flames and ionized gases showed fairly ordinary Ohmic conductivity, but at sufficient levels these currents saturated [4, 5, 6] at some maximum. In some of these experiments, the application of hundreds of volts failed to drive current beyond 100μA.

In a chemical plasma, the life span of ions may be quite short, but for the brief interval when they are allowed to travel separately, an external electric field can compel positive and negative charge carriers to drift in opposite directions. Provided that there is a semi-uniform plasma in all directions to provide replacements for the vacating ions, this process produces a current that appears quite linear (Ohmic) with respect to voltage. However, ion exchange at with an absorbing metal surface or at the edge of localized chemical activity breaks the chain of drifting ions.

A sufficiently strong electric field can drive away all of the charge carriers of one type in the vicinity of these regions, causing an abrupt change in the system's response to voltage. It is also well understood that a small fast charge carrier (like the electron) will impact a surface far more often than its slower counterparts; until its relative concentration has been depleted to bring their interaction with the surface into equilibrium. Both of these are phenomena that lead to the formation of a charged sheath in the vicinity of an absorbing surface.

These phenomena were famously used by Langmuir [7] as a means for measuring ion densities in plasmas using the geometrically simple probe that also bears his name [8, pp. 404]. Su and Lam's continuum model [9] for the "Langmuir sheath" represented substantial progress reflected in recent works modeling electrical currents in flat flames [10].

By the mid-twentieth century, these phenomena were being investigated to understand the chemical processes at work inside the flame [11, 12]. By 1969, Lawton and Weinberg had published a book describing these advances [13], and in 1997 Fialkov produced a detailed review of the substantial progress over the decades that followed [8].

Consensus has formed around much of the chemistry surrounding ions in methane flames [14, 15]. While honing simplified chemical mechanisms for conditions of engineering interest is still an area of active research [16], there seems to be no controversy regarding the identity of the dominant charge carriers. The positive ions are heavy molecules; usually HCO^+ and H_3O^+ with ratios depending on the conditions. The negative charge is accounted for primarily by the free electron, e^-, and O_2^-. A number of other chemically important charge carriers have been identified, but they do not persist in sufficient concentrations to contribute meaningfully to electrical currents.

Recent works have demonstrated substantial promise for the application of simplified models to the problem of predicting I-V characteristic features, but they indicate the need for validating data. A numerical model by Speelman et al. [17, 18] demonstrates important low-voltage features similar to the ones we identify in this study, and a highly simplified model by Xiong et al. shows similar promising agreement with counter-flow experiment [10]. These authors

identify the extreme asymmetry between the properties of the positive and negative charge carriers as the cause for what we refer to as partial saturation; an abrupt change in I-V characteristic that does not completely halt the flow of additional current. The Speelman model demonstrated an important sensitivity to transport properties, and the Xiong model exhibited a similar dependence on empirical tuning parameters. This serves to underscore the necessity for experimental data; especially given the inherently multi-dimensional nature of the system in question.

Though ion current sensing has found broad industrial application, the sensing approach proposed here is unusual in its attempt to deduce a multitude of system parameters from the shape of the current-voltage characteristic at low voltages. Since about the mid-twentieth century [19] and continuing to recent years [20, 21, 22] ion current sensing in IC engines is usually achieved by monitoring the evolution of ion currents subject to a steady excitation. Similar measurements have been used since the turn of the century to monitor combustion dynamics in gas turbine engines [23, 24], and sense precursors for lean-blowout in pulse engines [25]. Reported in 2013 to be among the most common methods for flame detection in the furnace and boiler industries [26], "flame rectification" sensors fundamentally perform a continuity check between electrodes. The most nuanced contemporary application is probably found in flame ionization detectors [15], wherein ions present in a hydrogen flame can be attributed to the carbon-laden molecules added from a sample.

Ion current investigations of this type have customarily been performed at voltages well over the 50VDC international standards established as safe for exposed industrial surfaces. Killovolt potentials have long been known to drive ionic winds sufficient to cause large-scale fluid mechanical effects [11, 27] that are still a topic of active study [28]. A number of studies have shown that intense electric fields can affect burning rate [29, 30, 31] with some interesting applications [32, 33]. In the present study, we will focus entirely on those voltages that can be easily produced by commercial-grade operational amplifiers.

2. Experiment

Measurements were conducted with an Oxweld C-67 cutting torch with a $\frac{1}{2}$-in two-piece fuel gas tip (named for the intended thickness of steel - not physical size). The tip burns premixed methane and oxygen from ten (10) preheat channels forming a total flow area approximately 7.5mm^2 (.012in^2). A room temperature gas flowing at 9.4L/min (20scfh) would have a velocity approximately 20m/s (67fps).

The flame geometry is commonly characterized as having "inner" and "outer" cones, describing the luminous zones forming at the fronts shown in Figure 2. The inner cone is an intensely luminous flame front anchored below the channel openings in conical shapes skewed by the step on the torch tip. The outer cone is a relatively faint luminous veil forming on the inner diameter of the step.

The system under investigation is represented diagrammatically in Figure 3. An oxy-fuel cutting torch was positioned over a steel coupon with internal

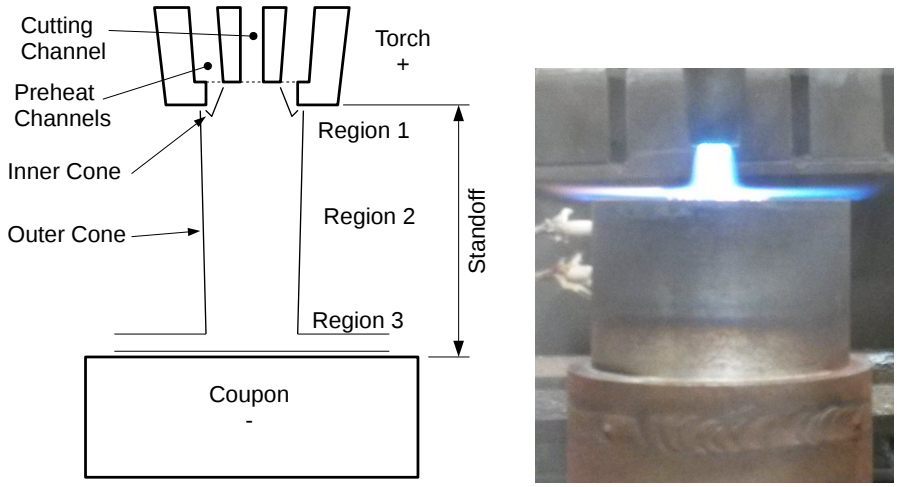

Figure 2: Cross section of the experimental arrangement with naming conventions labeled asside a photograph of the system. The coupon's embedded thermocouples are visible to the left, and the layer at which coolant is injected is visible from the dark-to-light oxidation boundary on the cylinder surface.

passages for coolant. The coupon and the table to which it was mounted were electrically grounded, while the torch was electrically isolated in its mounting by layers of Nomex and by lengths of Teflon tube replacing the standard conductive welding hoses.

The typical steel plate work piece was replaced with an SAE 4140 steel assembly forming a 54mm ($2\frac{1}{8}$in) diameter cylindrical coupon with internal cooling. A 1.3mm (.050in) gap formed a cooling cavity 19mm ($\frac{3}{4}$in) beneath the cylinder top surface, so that the assembly behaved as a disc thermally stabilized by bottom-side cooling. The flow rates of air (metered by critical orifice) and water (metered by rotameters) were adjusted to form a coolant mixture with highly tunable convection. The coolant mixture was adjusted until the surface temperature stabilized to the desired surface temperature independently of the disposition of the flame.

Direct measurement of the plate surface temperature was rendered impractical by the extreme temperatures, concerns about disturbing the flame, and highly radiative scale and small particulates well above the local plate temperature. Instead, two type-K thermocouples (visible in Figure 2) were welded on 3.2mm ($\frac{1}{8}$in) diameter ceramic rods and cemented in horizontal holes locating the beads at depths 6.4mm ($\frac{1}{4}$in) and 15.9mm ($\frac{5}{8}$in) from the top surface and 9.5mm (.373in) from the centerline. The surface temperature was calculated based on those embedded temperature measurements and coolant temperature measurements. While a detailed derivation of that model is outside of the scope of this paper, some discussion is afforded the method in Appendix A.

A rack-and-pinion height adjustment on the torch allowed for positioning in

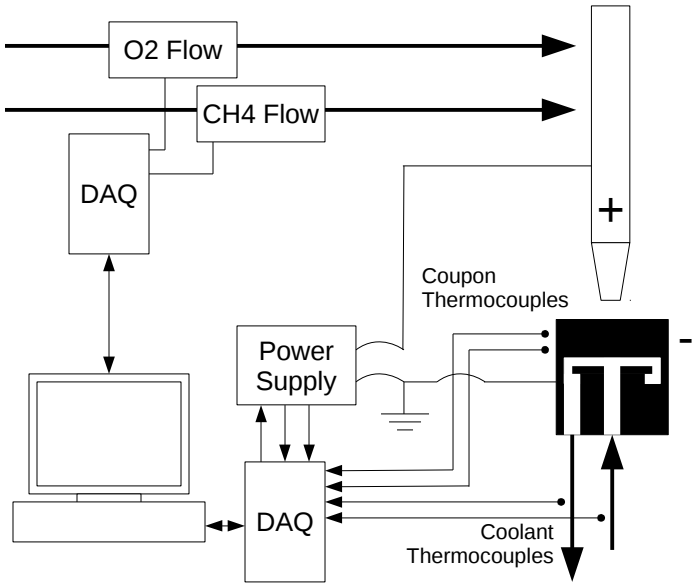

Figure 3: Experimental data collection diagram. Coolant and gas flow rates are regulated by metering valves not shown. Water flow rate is measured by rotameter and air flow rate is calculated from pressure at a critical orifice.

1.4mm (.05in) increments with approximately ±.25mm (.010-inch) uncertainty in the placement. Methane and oxygen were supplied from bottles, regulated to 10psig and 30psig respectively, and monitored with mechanical gauges. To prevent the thermally driven drift in flow rates commonly suffered by these torches, metering was accomplished in a separate room with needle valves. Oxygen and methane flow rates were measured by thermal mass flow meters accurate to .14L/min (.3scfh) and .07L/min (.15scfh) respectively.

A custom power supply was constructed to translate a 0V to 5V analog command from the data acquisition unit (DAQ) to -12.5V to 12.5V at the torch relative to the plate. The power supply returned two feedback measurements; one buffered analog voltage equal to the actual voltage applied and one proportional to the current. The output was scaled such that 1V indicated approximately 25μA. Prior to experiments, the power supply feedback was calibrated using a .1% 100kΩ shunt resistor and a precision multimeter.

Data were collected by interrogating the flame with a 5Hz ±10V triangle wave. The current was measured simultaneously with the voltage to produce a voltage-current characteristic. By collecting data with rising and falling voltages, it was possible to rule out dynamic or hysteresis effects.

To test for inadequacies in the torch isolation, measurements were first taken with no flame. Current in these conditions would indicate leakage bypassing the flame. No such current was detected.

We will adopt the naming conventions illustrated in Figure 2. Regions in space adjacent to the torch, in the outer cone, and adjacent to the plate are named regions 1, 2, and 3 respectively. The torch shall be regarded as positive, such that negative voltages imply that the torch is at a lower electrical potential than the coupon.

3. Results and Analysis

Figure 4 shows three I-V characteristic curves that are typical of these measurements. The shape of the curves naturally forms three regimes, which we number sequentially from left to right. The behavior in these regimes can be made to change drastically as the conditions are varied. The strongest changes are observed when manipulating the standoff and fuel-oxygen (F/O) ratio.

At negative voltages, the current has not yet completely saturated, but the discontinuity that separates regimes 1 and 2 forms what we will refer to as a *partial* saturation. As in the measurements of many authors before, positive saturation consistently appears as a kind of *soft* saturation that is not usually predicted by one-dimensional models.

For the purposes of discussing their dependencies on the many parameters we investigate here, we approximate the I-V characteristic with a piecewise linear curve;

$$V = \left\{ \begin{array}{c|c} (I - b_1)R_1 & I < I_{sat}^- \\ IR_2 + V_0 & I_{sat}^- < I < I_{sat}^+ \\ (I - b_3)R_3 & I_{sat}^+ < I \end{array} \right. \quad (1)$$

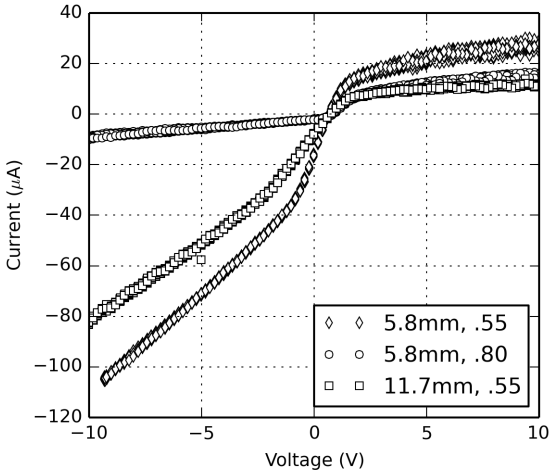

Figure 4: Current-voltage characteristics. Standoff and F/O ratio is listed in the legend. All conditions were at total 9.4L/min (20scfh) flow.

The parameters, R_1, R_2, R_3, b_1, b_3, and V_0, were determined by nonlinear least-squares regression on the I-V characteristic, and each fit was manually inspected for correct convergence.

When V and I are the voltage applied and the total current passing through the flame, R_1, R_2, and R_3 are the resistances forming the slopes in their respective regimes. The offset voltage, V_0, is the floating potential, while b_1 and b_3 are y-intercepts for the saturation regions bearing units of μA. The negative and positive saturation current levels, I_{sat}^- and I_{sat}^+, are determined by the points at which the line segments of equation 1 intersect,

$$I_{sat}^- = \frac{b_1 R_1 + V_0}{R_1 - R_2} \tag{2a}$$

$$I_{sat}^+ = \frac{b_3 R_3 + V_0}{R_3 - R_2}. \tag{2b}$$

The following analysis characterizes each regime by these characteristic parameters.

3.1. Regime 2: The Ohmic Regime

In the narrow regime in which no saturation has occurred, the flow of electrical current is limited by the resistance in the path forming the bridge between the plate and the torch. As we will discuss in some depth, this Ohmic behavior is actually present in all regimes, but dominates in regime 2.

This is most clearly demonstrated in Figure 5. Data were collected while holding flow and mixture constant while adjusting the standoff. In these condi-

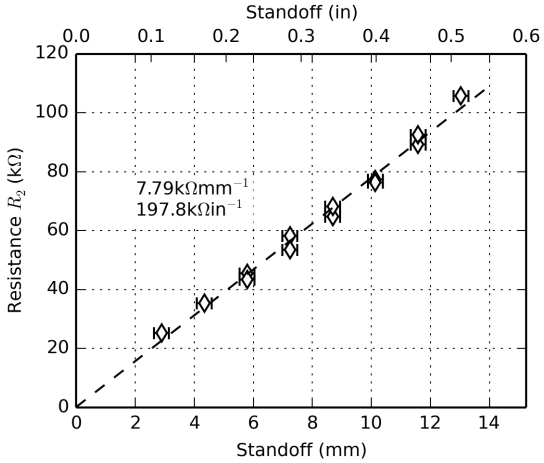

Figure 5: Ohmic regime resistance versus standoff with total flow 9.4L/min and F/O ratio 0.55.

tions, we see that the Ohmic regime resistance, R_2 is proportional to standoff. The effect is also visible in Figure 4.

Because the number and mobility of ions are strongly tied to the chemistry and temperature of the flame, we may expect to see a strong impact from the F/O ratio. Figure 6 shows the evolution of R_2 as the mixture was varied at three standoff distances.

Near stoichiometric conditions (0.50 F/O ratio for methane), R_2 is quite insensitive to mixture, but eventually trends strongly upwards with F/O ratio. The data of Figure 6 suggest a constant sensitivity of R_2 with respect to standoff; the distance between the curves is maintained even as F/O ratio is increased.

This contradicts the notion that mixture's impact on the resistivity is through the bulk resistivity of the outer cone. Instead, it appears that there is some other resistance in series that increases while the conductivity of the outer cone is held virtually constant. Physically, this coincides with the rich flame lifting from the torch tip. In fact, at the extreme cases above 0.80 F/O ratio, the flame separates entirely from the torch and stabilizes on the coupon surface.

3.2. Regime 1: Partial Negative Saturation

Electrical saturation in flames has been measured by countless authors, but it is somewhat unusual to see it appear as an abrupt transition to a new linear I-V curve. Xiong[10] and Speelman[17] both observed a similar behavior. The inflection in their models began as the diffusion velocity of electrons was reversed in total by the application of voltage. As Figure 4 suggests, this segment of the characteristic is strongly influenced by the fuel-oxygen ratio and weakly influenced by the standoff.

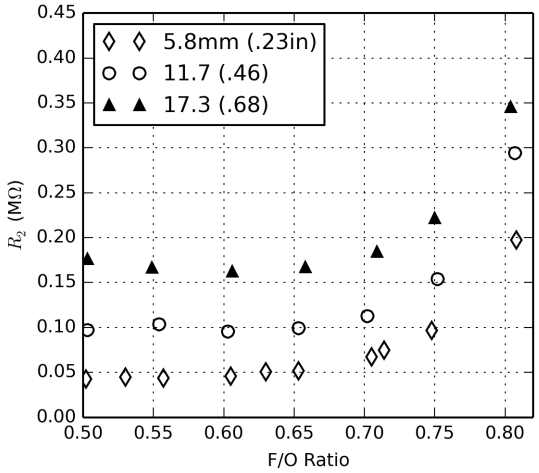

Figure 6: Ohmic regime resistance versus fuel-oxygen ratio (by volume) at various standoffs and 9.4L/min total flow.

Figure 7(a) shows the regime 1 resistance (R_1) plotted against F/O ratio for various standoff distances. Of course, ions are still making the journey between the torch to the coupon, so it seems reasonable to imagine that the offset between these data is caused by the increased path length. We separate the regime 1 resistance into two parts;

$$R_1 = R_1' + R_2, \tag{3}$$

the portion contributed by the bulk resistance of the flame, and the portion contributed by the partial saturation. When we inspect R_1', we see all standoff dependency vanish. Invariance with standoff seems to indicate that R_1' is a resistance that is localized to region 1 (the torch tip).

Further confirmation is found when we examine the impact of flow. Quite close to stoichiometric conditions (0.50 for methane), the inner cone length does not change perceptibly as flow is adjusted from 7.1L/min to 14.2L/min (15scfh to 30scfh). However, at rich mixtures, the inner cone can be made to elongate perceptibly, and Figure 8 shows a corresponding sensitivity in R_1'. The scatter in the rich data are due to the high sensitivity to small inconsistencies in F/O ratio.

From Figure 7, we also derive insight into the source of the offset that appears at rich mixtures in Figure 6. The behavior of R_1' is quite consistent with that of R_2. This could suggest the growth of a boundary between the flame and the torch as the inner cone elongates and begins to lift from the tip. If that were true, the same boundary should proportionally affect R_1' and R_2, but R_1' is unaffected by standoff.

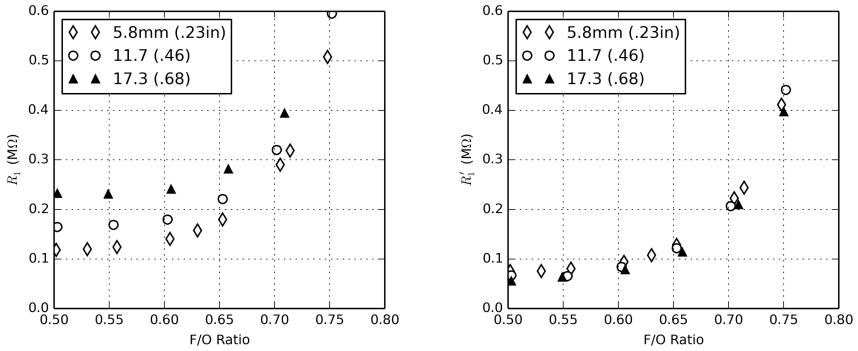

(a) (b)

Figure 7: Variations in (a) R_1 and (b) R_1' with F/O ratio and standoff. Flows were maintained at 9.4L/min (20scfh).

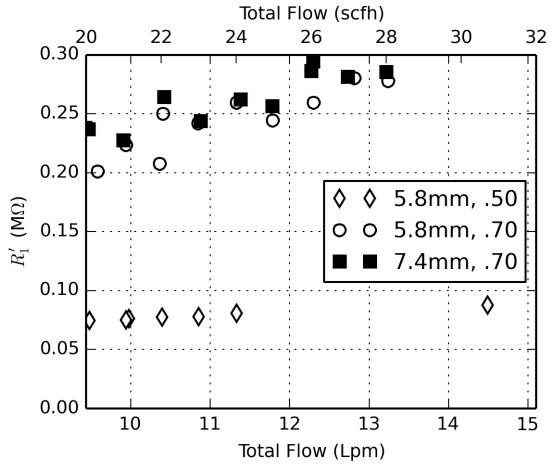

Figure 8: Variations in adjusted negative saturation resistance with flow at two F/O ratios.

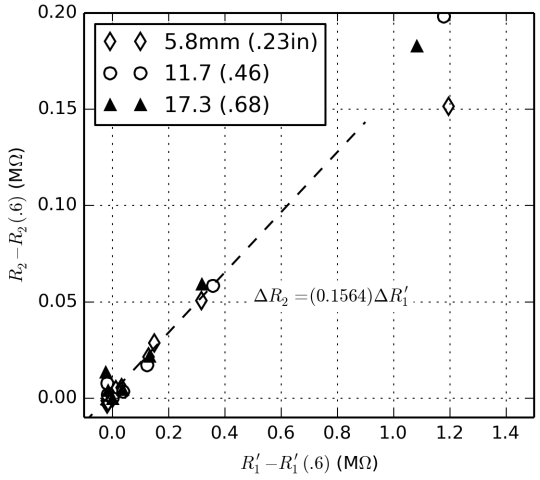

Figure 9: Ohmic resistance (R_2) plotted against the adjusted region 1 resistance (R_1').

In Figure 9 we name F/O ratio 0.60 as a reference state and observe a linear correlation between changes in the regime 1 resistance against regime 2 resistance. The scatter at high change in resistance is brought on by the extreme deformation of the I-V characteristic at ultra rich conditions (F/O ratio ≥ 0.85). In these cases the flame lifts completely off of the torch, negative saturation current approaches zero, the Ohmic region practically disappears, and the only significant feature is the positive saturation discussed below. The degradation in the quality of the regression is reflected in the increased scatter.

From this, we infer that the resistivity of the outer cone is not strongly a function of the F/O ratio. Instead, there is a series resistance in region 1 that changes with the inner cone length, causing drift in the regime 2 resistance.

Changing flow rates between 9.4L/min and 14.2L/min (20scfh and 30scfh) for fuel-oxygen mixtures 0.50 and 0.70 did not produced a significant change in regime 2 resistance. At F/O ratio of 0.70, Figure 6 shows an increase in R_1' of about 70kΩ, which is small enough to be contained in the cluster of data near the origin in Figure 9.

If the resistances determine how free ions are to move between regions, then the saturation currents should offer some insight into their abundance. Figure 10 shows that I_{sat}^- seems to exhibit an extremum near stoichiometric mixtures and declines in a semi-Gaussian manner at rich mixtures. The current at which saturation occurs is strongly influenced by deviations from a stoichiometric mixture much sooner than the resistances.

Disagreement in the data with high standoff may be interpreted as measurement error. At high standoff and fuel-oxygen mixtures near stoichiometric, R_1' becomes small relative to R_2 and $R_1 \approx R_2$. Visually, the inflection in the

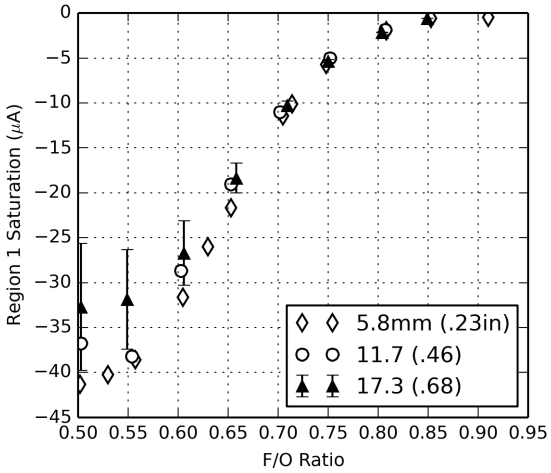

Figure 10: Variations in adjusted negative saturation resistance with flow at two F/O ratios. Error bars suppose a 5% error in resistance measurement.

I-V characteristic nearly vanishes and the calculation of I_{sat}^{-} from Equation 2 becomes singular. The error bars in Figure 10 show the rapid degradation in the measurement at the higher standoff.

Independence of saturation current on standoff further confirms that regime 1 phenomena are localized to region 1. The strong sensitivity near stoichiometric conditions is consistent with the idea that resistance should be most strongly linked to the mobility of the charge carriers, but that saturation currents will be most strongly linked with their rate of production. This presents the partial saturation current as a promising parameter by which to measure fuel-oxygen ratio.

3.3. Region 3: Positive Saturation

Perhaps the most definitive thing that can be recorded about regime 3 is that its behavior is far more erratic than that of regimes 1 and 2. Tests with various flow rates and plate temperatures see drastic and unrepeatable changes in R_3. While the other regimes of the I-V characteristic are stable and repeatable, the currents in regime 3 have changed suddenly by as much as 300% in a 5 second test during which all controlled parameters were held constant. These effects are almost certainly due to changes in the disposition of the coupon surface.

Figure 11 shows a series of regime 3 resistance measurements made with constant flow, standoff, and mixtures, but changing plate temperature. Here, we calculate R_3' in the same way we calculated R_1'.

$$R_3 = R_3' + R_2 \tag{4}$$

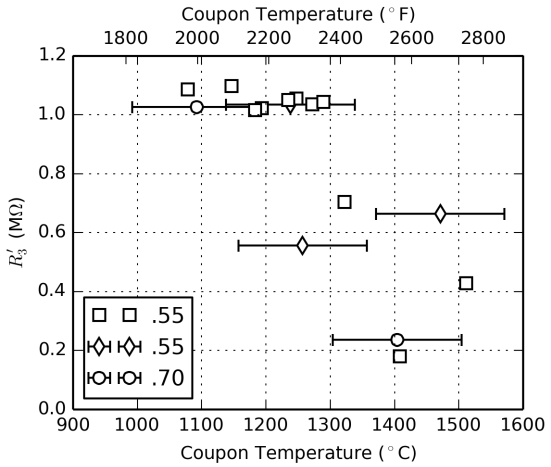

Figure 11: Regime 3 adjusted resistance with changes in coupon temperature for various conditions mixtures at 5.8mm (.23in) standoff. Error bars are omitted for squares to reduce clutter.

A detailed inspection of the I-V characteristic of most of these points reveal no observable difference until the plate temperature is allowed to approach the melting temperature of 4140 steel (about 1450°C 2600°F). During these tests, the surface character changes visually as a small pool of molten metal forms in the center of the plate. Tiny beads of molten metal (approximately 1mm diameter) have been found to freeze at the edge of the plate, and intermittent streams of radiating particulates can be observed leaving the pool. These conditions coincide with an abrupt reduction in regime 3 resistance.

It should be emphasized, however, that these data are extremely difficult to repeat. Figure 12 is a scatter plot of R_3' over some 70 tests at a wide range of conditions. The data seem to suggest an organized trend towards low resistance at the melting temperature of the coupon, but attempts to isolate patterns in specific data sets with controlled parameters give unexpected and often bizarre results.

The irregular nature of saturation in region 3 is almost certainly due to changes in the the surface condition of the coupon. Flaking due to oxidation, the momentary creation of surface roughness due to partial melting, and the deposition of frozen metal dust may all account for drastic unrepeatable changes in the microscale surface area. It is also important to note that the linear approximation for the saturation in this regime is not entirely satisfactory. In fact, careful inspection of some I-V curves shows evidence of curvature in the characteristic almost immediately after the current becomes positive.

There is some precedent for one-dimensional models exagerating the sharpness of the transition to saturation, which encourages the idea that the curvature

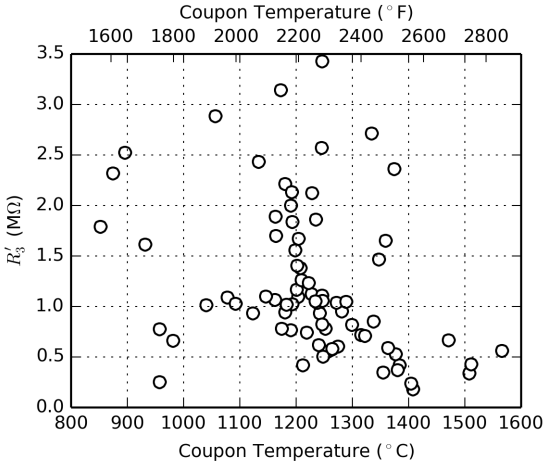

Figure 12: Regime 3 adjusted resistance scatter for a wide range of tests.

may be due to non-uniform saturation. These effects could also be attributed to mechanical degradations of the coupon surface (flaking, melting, freezing), or to the electric effects of chemical action at the coupon surface (like oxidation).

4. Conclusions

The outer cone exhibits a nearly uniform electrical resistivity along its length about 7.5kΩ per mm (190kΩ per inch). Changes to fuel-oxygen (F/O) ratio seem to affect the electrical characteristics at the inner cone, but they only weakly impact the outer cone. Flow rate did not have a strong effect at the precision data were collected.

Regime 1 partial saturation is characterized by a resistance (R_1') added in series with the bulk plasma resistance (R_2). This partial saturation seems to correspond to the abrupt discontinuities predicted separately by Speelman's and Xiong's models [18, 10].

While the regime 1 and 2 resistances exhibited little sensitivity to the F/O ratio near stoichiometric conditions, the negative saturation current was quite sensitive. From Figure 10, it appears that the negative partial saturation current enjoys insensitivity to standoff and excellent response to changes in F/O ratio. This is likely due to decline in the rate of generation of ions at rich conditions.

If standoff influences the negative saturation current or resistance (R_1'), it was not detectable in these experiments. One possible mechanism for such an influence is radiation from the plate causing additional heating of the tip. Though surface temperatures have not been shown to play a role in saturation in this study, the tip is also coupled to the incoming reactant temperature.

Regime 3 remains the most enigmatic, but it is clear that the condition of the coupon surface plays a major role. A linear fit to regime 3 may be inappropriate but offers parameters from which to identify trends. Flow and coupon temperature seem to impact regime 3, but the effects are entangled with tertiary effects that cause excessive scatter in these measurements. It seems most likely that small scale mechanical or chemical phenomena are also important.

With specific application to the potential for sensing in the metal working industry, we may infer that:

1. Torch-to-workpiece standoff is linked to the regime 2 resistance with the potential to correct for a secondary influence from F/O ratio;
2. Fuel-oxygen mixture is linked to the negative saturation current with little or no secondary influences;
3. Work surface temperature alone is not a good predictor for the system electrical characteristics presented here, but it does seem to be linked to the positive saturation characteristics;
4. Total gas flow rate has little or no influence in all of the regime 1 and 2 characteristics presented here.

At this juncture, there are a number of questions that present themselves for future investigation. Some previous studies on Bunsen flames shows that the outer cone has higher concentrations of ions in the layer where ambient oxidizer is entrained [8], but it is not necessary that this system will exhibit the same structure. Over the course of these measurements some tests exhibited relatively sharp transitions to saturation while others favored the "soft" transition to saturation. It seems intuitive that the outer cone electrical structure and the area of engagement between the flame and the coupon may play important roles in determining that transition.

It also remains to be demonstrated what happens to the I-V characteristic when the torch is engaged in a cut. The geometry of the coupon will be modified by the presence of a kerf, and the transonic flow of oxygen in the cutting channel visibly deforms both the inner and outer cones. There is reason to suspect that the cyclic accumulation and clearing of molten metal in the kerf may lead to corresponding cycles in the positive saturation regime (not entirely dissimilar to those observed in automotive applications). Such a possibility could offer an indication for the quality of the cut.

Acknowledgments

Credit and thanks are due to Dr. Valerian Nemchinsky. His advice proved quite valuable over the course of this investigation.

Appendix A. Plate Thermal Model

An analytical model for the temperature distribution in the plate was constructed by solving the Laplace equation in a cylindrical coordinate system.

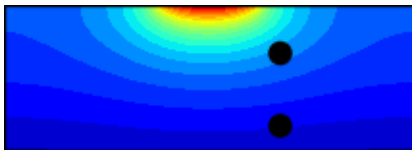

Figure A.13: Pseudo-color plate temperature distribution. Embedded thermocouple locations are marked with black dots.

Figure A.13 shows a pseudo-color representation of a 100-term Bessel function expansion solving the problem. The boundary conditions asserted an unknown but uniform heat addition over a 14.3mm ($\frac{9}{16}$in) diameter on the upper surface, an unknown convection coefficient to the coolant mixture below, and all other surfaces were insulated.

While the details of the derivation are outside the scope of this article, once evaluated, the surface temperature and heat conduction through the plate may be approximated by simple algebraic relationships.

$$t^{(2)} = T^{(2)} - T_C \tag{A.1a}$$

$$t^{(1)} = T^{(1)} - T_C \tag{A.1b}$$

$$\eta = 1 + \frac{t^{(2)}(1.894) - t^{(1)}(1.207)}{t^{(1)}(1.0032) - t^{(2)}(1.0005)} \tag{A.1c}$$

$$\Delta T = 1.4556 \left(t^{(1)} - t^{(2)} \right) \tag{A.1d}$$

$$T_{peak} = (3.903 + \eta)\Delta T + T_C \tag{A.1e}$$

$$\dot{Q} = \Delta T(4.2\text{W}/^\circ\text{C}) \tag{A.2}$$

Here, T_C is the average temperature of the coolant, $T^{(1)}$ and $T^{(2)}$ are temperatures at the upper and lower thermocouples, and T_{peak} is the surface temperature at the centerline. The dimensionless parameter, η, is the ratio of the total effective thermal resistance of the plate-coolant convection interface to that of the plate itself. Large η implies poor cooling, and small η implies good cooling. The temperature rise, ΔT, is a scale for the temperature drop across the entire plate. Note that equations A.1 are insensitive to the choice of units.

To validate the thermal model the coolant flow rates and temperatures were used to estimate the heat added to the coolant. To that end, vapor and liquid phase water were assumed to be in thermodynamic equilibrium in the air and a first-law analysis was performed. The heat predicted by equation A.2 was within 10% of that measured in the coolant at all operating conditions (typically about 1kW), and often closer. Since the surface temperatures are expected to be order of magnitude 1000°C, calculated temperatures were assumed accurate to ±100°C.

[1] Linde Company, The Oxyacetylene Handbook, 2nd Edition, Union Carbide Corp., New York, 1960.

[2] V. Bolobov, Conditions for the ignition of iron and carbon steel in oxygen, Combustion, Explosion, and Shock Waves 37 (3) (2001) 292–296.

[3] Timken Steel, 4140hw alloy steel technical data (2015).
URL `www.timkensteel.com`

[4] J. J. Thompson, Conduction of Electricity through Gases, 2nd Edition, Cambridge University Press, London, 1906.

[5] H. Wilson, The electrical conductivity and luminocity of flames containing salt vapours, Phil. Trans. R. Soc. Lond. A 216.

[6] H. Wilson, Electrical conductivity of flames, Reviews of Modern Physics 3 (1).

[7] I. Langmuir, Studies of electric discharges in gases at low pressures, General Electric Review 27 (12) (1924) 810.

[8] A. B. Fialkov, Investigations on ions in flames, Progress in Energy and Combustion Science 23 (1997) 399–528.

[9] C. H. Su, S. H. Lam, Continuum theory of spherical electrostatic probes, The Physics of Fluids 6 (10).

[10] Y. Xiong, D. G. Park, B. J. Lee, S. H. Chung, M. S. Cha, Dc field response of one-dimensional flames using an ionized layer model, Combustion and Flame 163 (2016) 317–325.

[11] H. Calcote, R. Pease, Electrical properties of flames, Industrial and Engineering Chemistry 43 (12).

[12] H. F. Calcote, Mechanisms for formation of ions in flames, Combustion and Flame 1 (4) (1957) 385–403.

[13] J. Lawton, F. J. Weinberg, Electrical aspects of combustion, Oxford: Clarendon Press, 1969.

[14] T. Pendersen, R. C. Brown, Simulation of electric field effects in premixed methane flames, Combustion and Flame 94 (1993) 433–448.

[15] T. Holm, Aspects of the mechanism of the flame ionization detector, Journal of Chromatography A 842 (1999) 221–227.

[16] R. Rao, D. Honnery, A simplified mechanism for the prediction of the ion current during methane oxidation in engine-like conditions, Combustion and Flame 162 (2015) 2928 – 2936.

[17] N. Speelman, L. de Goey, J. van Oijen, Development of a numerical model for the electric current in burner-stabilised methane-air flames, Combustion Theory and Modeling 19 (2) (2015) 159–187.

[18] N. Speelman, M. Kiefer, D. Markus, U. Maas, L. de Goey, J. van Oijen, Validation of a novel numerical model for the electrical currents in burner-stabilized methane-air flames, in: Proceedings of the Combustion Institute, Vol. 35, 2015, pp. 847–854.

[19] W. G. Rado, Characteristics of a plasma generated by combustion in a spark ignition engine, Journal of Applied Physics 46.

[20] N. Henein, W. Bryzik, A. Abdel-Rehim, A. Gupta, Characteristics of ion current signals in compression ignition and spark ignition engines, SAE International Journal of Engines 3 (1) (2010) 260–281.

[21] T. Badawy, A. Shrestha, N. Henein, Detection of combustion resonance using an ion current sensor in diesel engines, ASME Journal of Engineering for Gas Turbines and Power 134.

[22] R. Rao, D. Honnery, A study of the relationship between NOx and the ion current in a direct-injection diesel engine, Combustion and Flame 176 (2017) 309–317.

[23] B. T. Chorpening, J. D. Thortnton, E. D. Huckaby, K. J. Benson, Combustion oscillation monitoring using flame ionization in a turbulent premixed combustor, in: Proceedings of the ASME, Vol. 129, 2007, pp. 352–357.

[24] L. B. Peerlings, Manohar, V. N. Kornilov, P. de Goey, Flame ion generation rate as a measure of the flame thermo-acoustic response, Combustion and Flame 160 (2013) 2490–2496.

[25] F. Li, L. Xu, M. Du, L. Yang, Z. Cao, Ion current sensing-based lean blowout detection for a pulse combustor, Combustion and Flame 176 (2017) 263–271.

[26] E. Platvoet, C. Baukal, Process burners 101, CEP Magazine (2013) 35–39.

[27] J. Hu, B. Rivin, E. Sher, The effect of an electric field on the shape of co-flowing and candle-type methane-air flames, Experimental and Thermal Fluid Science 21 (2000) 124–133.

[28] J. Kuhl, T. Seeger, L. Zigan, S. Will, A. Leipertz, On the effect of ionic wind on structure and temperature of laminar premixed flames influenced by electric fields, Combustion and Flame 176 (2017) 391–399.

[29] S. Marcum, B. Ganguly, Electric-field-induced flame speed modification, Combustion and Flame 143 (2005) 27–36.

[30] J. van den Boom, A. Konnov, A. Verhasselt, V. Kornilov, L. de Goey, H. Nijmeijer, The effect of a DC electric field on the laminar burning velocity of premixed methane/air flames, in: Proceedings of the Combustion Institute, Vol. 32, 2009, pp. 1237–1244.

[31] M. Belhi, P. Domingo, P. Vervisch, Direct numerical simulation of the effect of an electric field on flame stability, Combustion and Flame 157 (2010) 2286–2297.

[32] S. Andreasson, E. Bemm, A. Larson, S. E. Nyholm, Evaluation of an electrothermal-chemical concept where propellant combustion is stimulated by conducting electric current through the flame, IEEE Transactions on Magnetics 41 (1) (2005) 338–343.

[33] G. Young, J. J. Koeck, N. T. Conlin, J. L. Sell, , G. A. Risha, Influence of an electric field on the burning behavior of solid fuels and propellants, Propellants Explosives Pyrotechnics 37 (2012) 122–130.